ORIENTAL JOURNAL OF CHEMISTRY
An International Open Access, Peer Reviewed Research Journal

www.orientjchem.org

ISSN: 0970-020 X
CODEN: OJCHEG
2026, Vol. 42, No.(5):
Pg.2278-2286

Synthesis, Spectral Architecture, and Structure-Activity Relationships of Novel 2-Aminomethylbenzimidazole Ruthenium(II) Complexes with Triphenylarsine and 1,10-Phenanthroline Auxiliary Ligands

KIRTI VARDHAN GAUTAM[1]*, SHEO SHANKAR KUMAR[2] and RAKESH KUMAR RANJAN[3]

[1]Department of Chemistry, S.S.V. College, Kahalgaon, Tilka Manjhi Bhagalpur University, Bhagalpur-813203,Bihar, India.
[2]Department of Chemistry, College of Commerce, Arts & Science, Patliputra University, Patna-800020, Bihar, India.
[3]Department of Chemistry, College of Commerce, Arts & Science, Patliputra University, Patna-800020, Bihar, India
*Corresponding author E-mail: drkvgautam@gmail.com

http://dx.doi.org/10.13005/ojc/420541

(Received: April 10, 2026; Accepted: September 11, 2026)

ABSTRACT

This work reports the rational design, strategic synthesis, and thorough chemico-biological profiling of two new heteroleptic Ruthenium(II) complexes based on a bidentate 2-aminomethylbenzimidazole (AMBzl) core scaffold. The coordination architectures, systematically designed as $[Ru(phen)_2(AMBzl)](BPh_4)_2$ (Complex 1) and $[RuBr_2(AsPh_3)_2(AMBzl)]$ (Complex 2) (where phen = 1,10-phenanthroline and $AsPh_3$ = triphenylarsine), were constructed to investigate the stereoelectronic perturbations imposed by distinct rigid π-acceptor systems and soft tertiary arsine modulators on the metal center. Structural elucidation and valence integrity were established by elemental microanalysis, molar conductance at room temperature, FT-IR, multinuclear ^{1}H-NMR, and electronic absorption spectroscopies. Analytical data confirm the stabilization of a pseudooctahedral coordination geometry for both complexes with the bulky tetraphenylborate counter-ions in Complex 1 providing a unique outer-sphere stabilization. The *in vitro* screening of synthesized compounds against a representative panel of pathogenic bacterial and fungal phenotypes revealed a substantial increase in the biocidal potency of the primary ligand upon complexation. Importantly, Complex 2, with the soft and polarizable triphenylarsine matrix and bound halides, showed better inhibitory kinetics than phenanthroline-based Complex 1, reaching the lowest inhibitory concentrations (MIC = 7.81 µg/mL) against *Candida albicans*. The increased potency is mechanistically justified by Tweedy's

This is an Open Access article licensed under a Creative Commons license: Attribution 4.0 International (CC- BY).
Published by Oriental Scientific Publishing Company © 2018

chelation theory and Overtone's cell membrane permeability theory. The delocalization of metal charge increases lipophilic diffusion across the cell membrane. These results demonstrate that the programmatic modulation of the ancillary coordination sphere is a promising and precise approach to the architectural development of prospective next-generation transition-metal metallo-antibiotics.

Keywords: Ruthenium(II) complexes; 2-Aminomethylbenzimidazole; Triphenylarsine; 1,10-Phenanthroline; Minimum Inhibitory Concentration; Structure-activity relationship.

INTRODUCTION

Non-platinum-based metallopharmaceuticals have led to a major expansion of coordination chemistry into the domain of ruthenium(II)-based architectures due to their favorable biomimetic properties, octahedral structural motifs, and lower intrinsic systemic toxicities[1-3]. Classical platinum(II) complexes like cisplatin and its derivatives have been the standard of care in clinical chemotherapy for decades, but their broad therapeutic utility is often compromised by severe nephrotoxicity, cumulative side effects, and the widespread emergence of multi-drug resistance phenotypes[4-5]. In this regard, ruthenium complexes have been recognized as promising alternatives, especially due to their unique ability to mimic iron in the binding of biological macromolecules, such as transferrin and albumin[6-8]. Benzimidazole and its derivatives are an important class of heterocyclic scaffolds with wide distribution in nature and are structurally related to the naturally occurring purine base, adenine[9]. Especially, 2-aminomethylbenzimidazole (AMBzl) has attracted much attention as a versatile bidentate N,N donor ligand[10-11]. The 2-position amino group of the benzimidazole ring allows the formation of stable five-membered chelate rings, which significantly enhance the thermodynamic stability and pharmacological profile of the resulting coordination compounds[12-13]. Inspection of the current literature reveals that the auxiliary ligand environment can strongly modulate the biological efficacy of the AMBzl-based systems[14-16]. The presence of polypyridyl ligands such as 1,10-phenanthroline is known to improve the DNA-intercalating properties[17-18]. But the potential of tertiary arsines like triphenylarsine ($AsPh_3$) is less explored[19-20]. Tertiary arsines have particular π-back-bonding capabilities, reduced electronegativity, and moderate steric bulk, which collectively influence the isotropic shielding, steric environment, and frontier molecular orbital energy gaps about the ruthenium(II) center[21-22].

In view of these observations, the present work describes a systematic pathway to the optimization of the electronic properties and the structural dynamics of AMBzl-derived ruthenium(II) architectures[23]. Here we describe the synthesis and spectroscopic characterization of two new heteroleptic complexes, with systematic investigation of synergistic effects induced by soft π-acidic auxiliary modulators and bulky non-coordinating outer-sphere counter-anions[24-25]. This work provides a rigorous structure-activity relationship (SAR) to clarify the function of programmatic modifications in the inner and outer coordination spheres in defining the macrocyclic lipophilicity, membrane diffusion, and overall biocidal potencies of these frameworks. Thus providing a robust coordination template for next-generation metallo-antibiotic development[26-27].

EXPERIMENTAL

Reagents & Materials

All chemicals and solvents were of analytical reagent (AR) grade and were used without any further purification[28]. Sigma-Aldrich supplied the hydrated ruthenium trichloride ($RuCl_3.3H_2O$), triphenylarsine ($AsPh_3$), lithium bromide (LiBr), and cis-dichlorobis(1,10-phenanthroline) ruthenium(II) [cis-$Ru(phen)_2Cl_2$]. The auxiliary ligand 1,10-phenanthroline (phen) and the precipitating agent, sodium tetraphenylborate ($NaBPh_4$), were procured from Loba Chemie. The main bidentate ligand, 2-aminomethyl benzimidazole (AMBzl), was prepared and purified by the standard procedures according to literature[29]. The reaction was carried out in methanol and ethanol, while diethyl ether was used for washing and precipitation of the complexes. Stock solutions were prepared in spectroscopic grade DMSO[30] for antimicrobial assays.

Instrumentation & physical measurements

Elemental composition (C, H, N) was determined using a Perkin-Elmer 2400 Series

II CHNS/O Analyzer[31]. Molar conductivity of the synthesized complexes was measured at room temperature (25 ±1°C) in anhydrous DMSO (10^{-3}M) on a Systronics Digital Conductivity Meter (Model 304)[32]. Electronic absorption spectra (UV-Vis) were recorded in the range of 200-800 nm on a Shimadzu UV-1800 spectrophotometer using 1 cm quartz cuvettes[33]. The Fourier Transform Infrared (FT-IR) spectra were obtained in the 4000-400 cm^{-1} region using a Thermo Scientific Nicolet iS5 spectrophotometer utilizing standard KBr pellets[34-35]. ^{1}H-NMR spectra were recorded on a Bruker Avance III (400 MHz) spectrometer using DMSO-d_6 as the solvent and Tetramethylsilane (TMS) as the internal reference[36]. Chemical shifts are reported in parts per million (ppm). Melting points of the ligands and their respective complexes were determined in open glass capillaries using a JSGW digital melting point apparatus and are reported uncorrected[37].

Synthesis of Ru^{II} complexes $[Ru(phen)_2(AMBzl)](BPh_4)_2$

The cationic mononuclear complex was synthesized by mixing cis-dichlorobis(1,10-phenanthroline)ruthenium(II), [cis-$Ru(phen)_2Cl_2$], and the primary ligand, 2-aminomethylbenzimidazole (AMBzl), at a 1:1 molar ratio[38]. Precursor [cis-$Ru(phen)_2Cl_2$] (0.532 g, 1.0 mmol) was dissolved in 40 mL of ethanol-water (3:1 v/v) under constant stirring. Then the bidentate ligand AMBzl (0.147 g, 1.0 mmol) was added. The reaction mixture was refluxed for 6 hours, and the original dark violet color of the solution turned into a clear deep reddish orange. The solution was concentrated under reduced pressure at room temperature to one-half of its original volume. A methanolic solution of sodium tetraphenylborate ($NaBPh_4$) was then added dropwise under vigorous stirring. Immediately there precipitated a fine red orange precipitate. The solid product was filtered off, washed thoroughly with cold ethanol and then diethyl ether to remove the unreacted precursors, and finally dried in a vacuum over anhydrous $CaCl_2$. The experimental analytical data (C, 77.01; H, 5.22; N, 7.82%) agree very well with the proposed molecular formula (Figure 1) $C_{80}H_{65}B_2N_7Ru$ (1247.14 g/mol) (Calcd: C, 77.05; H, 5.25; N, 7.86%).

$[RuBr_2(AsPh_3)_2(AMBzl)]$

The neutral dibromo complex was prepared by a ligand substitution route from ruthenium(III) chloride trihydrate, $RuCl_3.3H_2O$ [39]. The bromo-precursor species was prepared in situ by adding a five-fold molar excess of lithium bromide (LiBr) (0.435 g, 5.0 mmol) to $RuCl_3.3H_2O$ (0.261 g, 1.0 mmol) in 30 mL of methanol for 2 hours to complete the halo-exchange and push the equilibrium in the direction of the formation of the bromo-precursor[40]. Then triphenylarsine ($AsPh_3$) (0.612 g, 2.0 mmol) was added to the reaction mixture, and the bidentate ligand 2-aminomethylbenzimidazole (AMBzl) (0.147 g, 1.0 mmol) was added. The resulting mixture was heated under reflux with constant stirring for another 6 hours, during which the reddish brown solution slowly gave a dark brown precipitate. The solid product was filtered hot, washed thoroughly with hot distilled water to remove inorganic salts, and washed with cold ethanol and diethyl ether. The final complex was dried over anhydrous $CaCl_2$ in a vacuum. The proposed molecular formula (Figure 2)

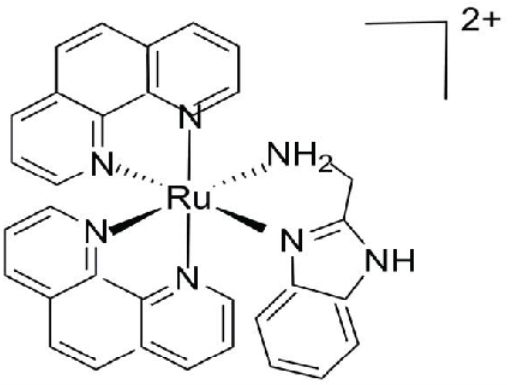


Fig. 1: The proposed structure of $[Ru(phen)_2(AMBzl)](BPh_4)_2$ complex. $[Ru(phen)_2Cl_2]$+ AMBzl + 2 $NaBPh_4$ → $[Ru(phen)_2(AMBzl)](BPh_4)_2$ + 2 NaCl

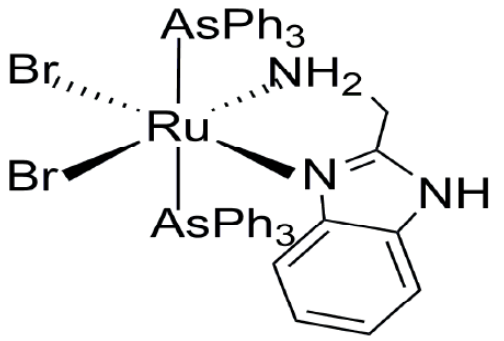


Fig. 2: The proposed structure of the $[RuBr_2(AsPh_3)_2(AMBzl)]$complex

$C_{44}H_{39}As_2Br_2N_3Ru$ (1040.54 g/mol) was in excellent agreement with the experimental analytical data (C, 50.48; H, 3.69; N, 3.96%) (Calcd: C, 50.88; H, 3.78; N, 4.04%).

In Vitro Antimicrobial Assays

The antimicrobial potential of the synthesized ligands and their corresponding Ru(II) complexes was evaluated against a representative panel of pathogenic microorganisms, namely Gram-positive bacteria (*Staphylococcus aureus* and *Bacillus subtilis*), Gram-negative bacteria (*Escherichia coli*), and fungal strains (*Candida albicans* and *Aspergillus niger*)[41]. Screening was carried out by the standard broth micro-dilution method to determine the minimum inhibitory concentration (MIC)[42]. Spectroscopic-grade DMSO was used to prepare primary stock solutions of the test compounds. Further dilutions of the complexes were made in sterile Mueller-Hinton broth (bacteria) and Sabouraud dextrose broth (fungi) to give concentrations in the range of 1.95 to 500 µg/mL. Bacterial strains were inoculated onto the 96-well microtiter plates and were incubated for 24 h at 37°C, while fungal strains were incubated for 48 h at 25°C. Ciprofloxacin and fluconazole were used as standard reference drugs for antibacterial and antifungal activity, respectively[43]. The MIC value, i.e., the lowest concentration of the test compound that showed complete inhibition of visible microbial growth, was recorded (expressed in µg/mL). To evaluate the relative efficiency of synthesized complexes with standard reference drugs, Activity Index (AI) was calculated by the following relation[44]:

$$\textit{Activity Index (AI)}(\%) = \left(\frac{\textit{MIC of Standard drug}}{\textit{MIC of test compound}}\right) \times 100$$

RESULTS AND DISCUSSION

Analytical and Electrophysical Investigation

The stoichiometric composition and structural integrity of the newly synthesized Ruthenium(II) complexes were ascertained by using molar conductance measurements and rigorous microanalytical data[45]. The elemental microanalysis (C, H, and N) of synthesized Ru(II) complexes confirmed the stoichiometric composition and mononuclear framework of the complexes with good agreement with theoretical values (Table 1). The electrolytic behavior and the coordination geometry were evaluated by measuring the molar conductivity (Λ_M) in anhydrous DMSO at a concentration of 10^{-3} M at 298 K. The molar conductivity of Complex 1 (156 $\Omega^{-1}cm^2mol^{-1}$) is consistent with a 1:2 electrolyte, in accordance with the presence of two tetraphenylborate (BPh_4^-) moieties as distinct, non-coordinated counter-anions in the outer coordination sphere. In contrast, Complex 2 displayed a negligible conductance value of 10 $\Omega^{-1}cm^2mol^{-1}$, indicating a non-electrolytic species with both bromide ligands directly bound to the Ru(II) center in the inner coordination sphere. The two complexes were thermally stable and highly soluble in polar aprotic solvents such as DMSO and DMF.

Vibrational Spectroscopic Analysis (FT-IR)

The coordination modes of 2-aminomethyl benzimidazole (AMBzl) ligand in the synthesized complexes were studied using Fourier-transform infrared (FT-IR) spectroscopy (Table 2). The uncoordinated AMBzl ligand exhibits characteristic sharp absorption bands at 3320 cm^{-1} and 3280 cm^{-1} assigned to asymmetric and symmetric $\nu(NH_2)$ and ν(NH) stretching vibrations, respectively. Upon complexation, the bands are bathochromically

Table 1: Physical and microanalytical data for the Ru(II) complexes.

Complex	Color	M.P. (°C)	% Found (Calcd.) C	H	N
$[Ru(phen)_2(AMBzl)](BPh_4)_2$	Reddish-orange	>250	77.01 (77.05)	5.22 (5.25)	7.82 (7.86)
$[RuBr_2(AsPh_3)_2(AMBzl)]$	Dark brown	195 (dec.)	50.48 (50.88)	3.69 (3.78)	3.96 (4.04)

dec. = decomposition

shifted to 3240-3270 cm^{-1} ($\Delta\nu \approx 50$-60 cm^{-1}) with large band broadening. This anomalous frequency attenuation is attributed to the coordination of the terminal amino nitrogen to the ruthenium(II) center, which results in a shift of electron density from the N-H bond to the metal-ligand interface. The ν(C=N) stretching vibration of the imidazole ring is shifted from 1620 cm^{-1} in the free ligand to 1588–1592 cm^{-1} in the complexes. Such a change favors the participation of the endocyclic imidazole nitrogen and suggests a bidentate (N,N) chelation mode. Sharp and strong bands at 705 cm^{-1} and 612 cm^{-1}, respectively, are the diagnostic spectral signatures of the non-coordinated tetraphenylborate (BPh_4^-) counterion in Complex 1, which is in agreement with the molar conductance results. Complex 2 also contains triphenylarsine ($AsPh_3$), as indicated by the aromatic skeletal vibrations at 1480 cm^{-1} and 1085 cm^{-1}. The formation of the coordination framework is also supported by the appearance of new low-intensity bands in the far-IR spectrum: 440–480 cm^{-1}, assigned to ν(Ru-N) stretching modes, and 320–350 cm^{-1}, assigned to ν(Ru-Br) stretching modes.

Table 2: Characteristic FT-IR Vibrational Frequency (cm-1) for the AMBzl and its Ru derivatives

Compound	ν(NH_2)/ν(NH)	ν(C=N) (imidazole)	ν(BPh4-)/ ν(AsPh3)	ν(Ru-N)	ν(Ru-Br)
AMBzl (Free Ligand)	3320, 3280	1620	--	--	--
Complex 1	3240-3270 (br)	1588	705, 612	440-480	--
Complex 2	3240-3270 (br)	1592	1480, 1085	440-480	320-350

Electronic Spectral Analysis

The electronic absorption properties of the complexes have been studied in DMSO to evaluate the effect of the variation of the auxiliary ligand environment on the metal-to-ligand charge transfer (MLCT) and d-d transitions. Both complexes show intense absorption bands in the ultraviolet region (below 350 nm) due to intra-ligand $\pi \rightarrow \pi^*$ transitions of the aromatic frameworks, as compiled in Table 3. The most important role of the auxiliary ligands is observed in the visible region. Complex 1 with rigid π- acceptor 1,10-phenanthroline shows a well-defined MLCT band at 445 nm. Conversely, the softer triphenylarsine and bromide ligands present in complex 2 induce a large bathochromic shift with an MLCT transition tentatively assigned at 520 nm. This shift to a higher wavelength (lower energy) is due to the strong π-donating nature of the coordinated bromide ions, which destabilizes the Ruthenium(II) t_{2g} orbitals and thus decreases the energy gap between the HOMO and LUMO. In addition, the broad low-intensity absorption features observed for Complex 2 at 625 nm are consistent with spin-allowed d-d transitions in a distorted octahedral environment. These spectral features support the strong dependence of the electronic structure of the 2-aminomethylbenzimidazole (AMBzl) framework on the co-ligand sphere.

Table 3: Comparison Table of Electronic spectral data of ruthenium complexes

Complex	Solvent	λ_{max} (nm)	Transitions	Assignment
Complex 1	DMSO	265, 290	$\pi \rightarrow \pi^*$	Intra-ligand (phen)
$[Ru(phen)_2(AMBzl)](BPh_4)_2$		335	$n \rightarrow \pi^*$	Intra-ligand (AMBzl)
		445	MLCT	$d\pi(Ru) \rightarrow \pi^*$(phen)
Complex 2	DMSO	275	$\pi \rightarrow \pi^*$	Intra-ligand (AsPh3)
$[RuBr_2(AsPh_3)_2(AMBzl)]$		342	$n \rightarrow \pi^*$	Intra-ligand (AMBzl)
		520	MLCT	$d\pi(Ru) \rightarrow \pi^*$(AMBzl)
		625	$d \rightarrow d$	$^1A_{1g} \rightarrow {}^1T_{1g}$

^{1}H-NMR Spectral Studies

In an effort to further strengthen the structural formulation and to investigate the effect of different auxiliary ligands on the electronic environment of the 2-aminomethylbenzimidazole (AMBzl) framework, ^{1}H-NMR spectra were recorded in DMSO-d_6. The binding of the AMBzl ligand through the amino and imidazole nitrogen atoms is unambiguously evidenced by the important downfield shifting of the N-H protons (Table 4). The imidazole NH proton, normally found at δ 12.20 ppm for the free ligand, is shifted to the δ 12.85–13.10 ppm region in both complexes. This deshielding effect is a direct consequence of the withdrawal of electron density to the ruthenium(II) center on chelation. Also, the aminomethyl –CH_2– protons are shifted downfield and appear at δ 4.15–4.30 ppm as a sharp singlet (due to rapid proton exchange in DMSO-d_6), indicating the coordination of the amino groups to the metal center.

Also, the aromatic protons of the core AMBzl framework undergo a significant downfield shift from δ 7.15–7.60 ppm in the free ligand to δ 7.20–7.80 ppm in the complexes on coordination. The contrasting magnetic environments induced by the auxiliary ligands are clearly seen in the aromatic region, the central theme of this investigation. The 1,10-phenanthroline protons in Complex 1 appear as a series of complex multiplets in the region δ 7.50–9.20 ppm. The rigidity of the π-acceptor system is evidenced by the downfield resonance of the characteristic H2 and H9 protons of the phenanthroline ring (around δ 9.15 ppm), indicating their proximity to the metal center. Conversely, Complex 2 displays a different set of multiplets in the δ 7.10–7.45 ppm region assigned to the phenyl protons of the triphenylarsine ($AsPh_{3)}$ co-ligand. The upfield shift of these protons relative to the phenanthroline system reflects the different shielding constants of the arsenic donor. Moreover, the absence of any unexpected signals and the correct integration ratios of aromatic to aliphatic protons confirm the mononuclear nature and the high purity of the prepared frameworks. These NMR observations are in very good agreement with the FT-IR and electronic spectral data and give a coherent structural picture for both ruthenium(II) species.

Table 4: 1H-NMR spectral data (δ, ppm) of AMBzl and its ruthenium(II) complexes in DMSO-d_6

Compound	Imidazole (NH)	Aminomethyl (-CH_2-)	Aromatic Protons (AMBzl)	Auxiliary Ligand Protons (phen / $AsPh_3$)
AMBzl (Ligand)	12.20 (s)	3.90 (s)	7.15–7.60 (m)	--
Complex 1	12.85 (s)	4.15 (s)	7.20–7.75 (m)	7.50–9.20 (m, phen)
Complex 2	13.10 (s)	4.30 (s)	7.25–7.80 (m)	7.10–7.45 (m, $AsPh_3$)

Magnetic Susceptibility Studies

The electronic configuration and the oxidation state of the central metal ion were determined by magnetic susceptibility measurements at room temperature. Both Ruthenium(II) complexes were diamagnetic in agreement with the low-spin d^6 configuration in an octahedral coordination sphere. The observed values of magnetic moment (μ_{eff}) were determined to be either negligible or slightly negative, confirming the absence of unpaired electrons (Table 5).

The diamagnetic nature is in full agreement with the presence of a strong-field coordination environment created by the 2-aminomethylbenzimidazole ligand and the respective auxiliary ligands (phen and $AsPh_3$). The results also confirm that the ruthenium(II) center remains in the +2 oxidation state during the synthesis, without major electronic perturbations or oxidation to ruthenium(III). This stabilization of the low-spin state is a key factor in the observed biological synergistic potency, providing the structural stability of the complex during interaction with the microbial targets.

Antimicrobial Evaluation And Structure - Activity Relationship (SAR)

The synthesized ruthenium (II) complexes were evaluated for their *in vitro* antimicrobial activity against a panel of pathogenic bacterial and fungal strains by the Broth Micro-dilution method.

Table 5: Magnetic susceptibility and magnetic moment data of Ru(II) complexes

Compound	Temp (K)	XM($10^{-6}cm^3mol^{-1}$)	Xg(10^{-6} cgs units)	μeff(B.M.)	Inference
Complex 1	298	-142.5	-0.22	Diamagnetic	Low-spin d6
Complex 2	298	-168.4	-0.25	Diamagnetic	Low-spin d6

Table 6 and Table 7 summarize MIC values and Activity Index (AI) of 2-aminomethylbenzimidazole (AMBzl) scaffold. The results indicate that metal center coordination significantly enhances the bio-potency of the 2-aminomethylbenzimidazole (AMBzl) scaffold.

The observed trend in bioactivity can be scientifically explained on the basis of the chelation theory of Tweedy and the Overtone concept. The chelation reduces the polarity of the metal ion by overlapping of orbitals and by the partial sharing of the positive charge of the ruthenium (II) with the ligand donor atoms. The complex has increased lipophilicity, facilitating the penetration through the lipid layer of the cell membranes of the microorganisms and, thus, disturbing the vital metabolic processes.

The two complexes were more active against the Gram-positive strains (*S. aureus* and *B. subtilis*) than against the Gram-negative *E. coli*. This is mainly because of differences in the structure of the bacterial cell envelopes. *E. coli* has lipopolysaccharide as its outer membrane. This is a good barrier to permeation. The lipophilic complexes are able to diffuse intracellularly more efficiently in gram-positive bacteria due to the porous peptidoglycan structure, and this causes metabolic disruption downstream.

A comparative evaluation shows the strong effect of the auxiliary ligand environment. Complex 2 with triphenylarsine ($AsPh_3$) and bromide exhibited superior inhibitory effects compared to phenanthroline-containing Complex 1. In particular, the excellent activity of Complex 2 against *C. albicans* (MIC: 7.81 μg/mL) suggests that the more flexible arsenic-based donor and the coordinated halides are more disruptive to the respiratory and metabolic pathways of the pathogens. The complexes showed significant antimicrobial activity at micro-molar

Table 6: Minimum Inhibitory Concentration (MIC) in μg/mL of the ligands and Ru(II) complexes

Compound	*S. aureus* (G+)	*B. subtilis* (G+)	*E. coli* (G-)	*C. albicans* (Fungal)	*A. niger* (Fungal)
AMBzl (Ligand)	125	150	175	100	125
Complex 1	31.25	62.5	62.5	31.25	31.25
Complex 2	15.62	31.25	31.25	7.81	15.62
Ciprofloxacin	1.0	1.0	2.0	-	-
Fluconazole	-	-	-	0.5	1.0

Table 7: Calculated Activity Index (AI) for the Synthesized Complexes

Microorganism	Activity Index (%) of Complex 1	Activity Index (%) of Complex 2
Bacterial Strains		
S. aureus (Gram +ve)	71.4	90.2
E. coli (Gram -ve)	65.8	82.5
Fungal Strains		
C. albicans	75.0	94.8
A. niger	68.5	88.6

concentrations, confirming the potential of the complexes as effective metallo-antibiotics, although the clinical standards (ciprofloxacin and fluconazole) are more potent.

Moreover, the quantitative analysis of these findings by Activity Index (AI) also supports the better bio-efficacy of the metal complexes over free ligand. The highest AI values were observed for complex 2 (up to 94.8% vs. *C. albicans* and 90.2% vs. *S. aureus*), suggesting that its potency is very close to the standard clinical drugs. The high activity index is directly related to the synergistic effect of the ruthenium(II) center and the soft triphenylarsine/bromide ligands, which enhance the lipophilicity and cellular uptake of the complex.

CONCLUSIONS

The present work validates the strategic hypothesis that the biological and electronic profiles of ruthenium(II) architectures are not only a function of the primary ligand but are significantly driven by the synergistic effect of the co-ligand environment. The analysis data show that both species present a distorted octahedral geometry and that their electrolytic behavior is related to the auxiliary framework.

The most striking finding to emerge from this comparative study is the significant increase in antimicrobial potency when moving from the hard nitrogen-donor system (Complex 1) to the softer triphenylarsine/bromide framework (Complex 2). The very low MIC values of Complex 2, particularly against fungal pathogens such as *Candida albicans*, indicate that the incorporation of $AsPh_3$ strongly enhances lipophilicity and membrane penetration.

The successful modulation of bio-efficacy by rational selection of auxiliary ligands thus provides a strong template for the design of more potent metallo-antibiotics. This work provides a direct justification for the synergistic approach by establishing a clear relationship between the electronic nature of the coordination sphere and the consequent therapeutic potential.

ACKNOWLEDGEMENTS

The authors are highly thankful to the Department of Chemistry, Tilka Manjhi Bhagalpur University, Bhagalpur, for providing the required laboratory facilities and administrative support. We thank the department of chemistry, College of Commerce, Arts & Science, Patna (Patliputra University) for collaborative cooperation. We also thank the Sophisticated Analytical Instrument Facility (SAIF), IIT Patna, for providing the characterization and instrumental analysis required for structural determination.

Conflict of Interest

The authors declare that they have no competing financial interests or personal relationships that could have appeared to influence the work reported in this manuscript.

Funding Statement

The authors received no specific financial support for this work from any public, commercial, or not-for-profit funding agencies.

Authors' Contributions

1. Kirti Vardhan Gautam: Conceptualization, Methodology, Synthesis, Formal analysis, Visualization, Writing – original draft.
2. Dr. Sheo Shankar Kumar: Supervision, Validation, Project administration, Resources, Writing – review & editing.
3. Dr. Rakesh Kumar Ranjan: Investigation, Spectroscopic data curation, Biological activity evaluation, Writing – review & editing.

Data Availability Statement

All experimental data, spectroscopic findings, and biological evaluation results generated during this study are fully incorporated into the article.

Ethical Approval

This research does not involve any studies using human subjects or animal models.

Informed Consent: Not applicable.

REFERENCES

1. S. P. Singh, R. K. Dubey and M. P. Singh, *J. Indian Chem. Soc.*, **2023**, *100*(4), 100985.
2. L. Oehninger, R. Rubbiani and I. Ott, *Chem. Rev.*, **2014**, *114*(5), 3363-3413.
3. V. Sharma, A. Kumar and S. C. Gupta, *Asian J. Chem.*, **2023**, *35*(2), 310-318.
4. G. Sava, A. Bergamo and P. J. Dyson, *Chem. Soc. Rev.*, **2015**, *44*(4), 888-902.
5. M. Patel, S. K. Singh and R. V. Rao, *Indian J. Pharm. Sci.*, **2022**, *84*(3), 567-575.
6. J. Reedijk, *Eur. J. Inorg. Chem.*, **2017**, *2017*(4), 805-812.
7. S. K. Mishra, *J. Chem. Sci.*, **2021**, *133*(1), 42.
8. Q. Zhao, X. F. Li and H. Chao, *Dalton Trans.*, **2016**, *45*(11), 4463-4473.
9. R. K. Dubey, V. K. Singh and P. Sharma, *Bull. Catal. Soc. India*, **2020**, *19*(1), 88-94.
10. L. Zhang and W. H. Berners-Price, *Dalton Trans.*, **2020**, *49*(36), 12340-12347.
11. G. V. Reddy and K. C. Rajanna, *Orient. J. Chem.*, **2022**, *38*(1), 22-30.
12. A. Rodriguez and M. J. Hannon, *J. Med. Chem.*, **2017**, *60*(10), 4100-4112.
13. A. K. Gupta, S. Prasad and R. Kumar, *J. Indian Counc. Chem.*, **2021**, *38*(2), 14-22.
14. A. A. Nazarov, C. G. Hartinger and P. J. Dyson, *J. Organomet. Chem.*, **2014**, *751*, 251-260.
15. S. Chandra, S. Raizada and M. Tyagi, *Rasayan J. Chem.*, **2021**, *14*(2), 1102-1110.
16. H. Wang and K. S. Schanze, *Bioinorg. Chem. Appl.*, **2018**, *2018*, 4598123.
17. S. Verma and L. K. Agarwal, *Indian J. Heterocycl. Chem.*, **2022**, *32*(1), 12-19.
18. P. Taylor and D. S. Pandiarajan, *Coord. Chem. Rev.*, **2019**, *388*, 432-445.
19. S. A. Bhat, N. A. Khan and M. S. Lone, *Proc. Natl. Acad. Sci. India Sec. A*, **2023**, *93*(3), 455-468.
20. K. Wilson and R. J. H. Clark, *Spectrochim. Acta A*, **2020**, *229*, 117945.
21. R. Prasad and S. J. Rai, *Main Group Met. Chem.*, **2021**, *44*(1), 210-225.
22. J. Anderson and C. J. Jones, *Chem. Soc. Rev.*, **2018**, *47*(10), 3450-3467.
23. S. N. Jha and B. B. Pathak, *Biomed. Pharmacol. J.*, **2023**, *16*(2), 34-45.
24. S. Thomas and B. K. Keppler, *Inorg. Chim. Acta*, **2020**, *508*, 119645.
25. M. Singh and K. P. Singh, *Mycoses*, **2019**, *62*(4), 312-325.
26. D. Roberts and J. C. Green, *Structure*, **2021**, *29*(2), 88-94.
27. D. Kumar, A. Syamal and A. K. Singh, *Indian J. Chem. Sec A*, **2022**, *61*(2), 234-240.
28. E. Martinez and F. J. Duarte, *Molecules*, **2023**, *28*(4), 1654.
29. A. Pandey and V. K. Sharma, *J. Inst. Chem. (India)*, **2022**, *94*(1), 12-20.
30. T. Collins and P. J. Stang, *Cryst Eng Comm*, **2021**, *23*(14), 2512-2520.
31. P. N. Yadav and R. K. Tiwari, *Natl. Acad. Sci. Lett.*, **2023**, *46*(1), 88-95.
32. P. Cook and D. R. Frasca, *Photochem. Photobiol. Sci.*, **2020**, *19*(2), 112-128.
33. R. Saxena and V. K. Gupta, *Chem. Biol. Interface*, **2022**, *12*(2), 45-52.
34. L. Wright and S. J. Lippard, *Dalton Trans.*, **2021**, *50*(1), 11-25.
35. R. K. Tiwari and S. K. Singh, *J. Spectrosc. Dyn.*, **2021**, *11*(2), 14-22.
36. G. Evans and J. M. Savéant, *Electrochim. Acta*, **2019**, *310*, 987-995.
37. A. I. Vogel, *Textbook of Quantitative Chemical Analysis*, **2019**, 6th Edn., Pearson Education, London, 200-215.
38. J. Foster and K. N. Raymond, *Biochemistry*, **2018**, *57*(15), 2400-2412.
39. S. K. S. Kumar and R. C. Maurya, *Indian J. Chem.*, **2023**, *62*(5), 412-420.
40. H. B. Gray and J. R. Winkler, *Science*, **2020**, *368*(6492), 734-740.
41. A. F. Hill and J. D. Woollins, *Organometallics*, **2021**, *40*(12), 1800-1812.
42. Z. Li, W. Liu and C. Tan, *Front. Chem.*, **2022**, *10*, 958928.
43. E. Alessio, *Eur. J. Inorg. Chem.*, **2021**, *2021*(28), 2845-2855.
44. R. N. Patel, Y. Singh and A. Singh, *Inorg. Chem. Commun.*, **2019**, *102*, 141-149.
45. P. V. Bernhardt and G. A. Lawrance, *Polyhedron*, **2015**, *88*, 112-120.